energies

MDPI

Article

Dynamic Thermal Features of Insulated Blocks: Actual Behavior and Myths

Marta Cianfrini [1], Roberto de Lieto Vollaro [1] and Emanuele Habib [2,*]

[1] Dipartimento di Ingegneria Meccanica e Industriale, Università degli Studi Roma Tre, Via della Vasca Navale 79, 00146 Rome, Italy; marta.cianfrini@uniroma3.it (M.C.); roberto.delietovollaro@uniroma3.it (R.d.L.V.)

[2] Dipartimento di Ingegneria Astronautica, Elettrica ed Energetica, Sapienza Università di Roma, Via Eudossiana 18, 00184 Rome, Italy

* Correspondence: emanuele.habib@uniroma1.it; Tel.: +39-06-4458-5349

Received: 19 October 2017; Accepted: 7 November 2017; Published: 9 November 2017

Abstract: The latest updates in the European directive on energy performance of buildings have introduced the fundamental "nearly zero-energy building (NZEB)" concept. Thus, a special focus needs to be addressed to the thermal performance of building envelopes, especially concerning the role played by thermal inertia in the energy requirements for cooling applications. In fact, a high thermal inertia of the outer walls results in a mitigation of the daily heat wave, which reduces the cooling peak load and the related energy demand. The common assumption that high mass means high thermal inertia typically leads to the use of high-mass blocks. Numerical and experimental studies on thermal inertia of hollow envelope components have not confirmed this general assumption, even though no systematic analysis is readily available in the open literature. Yet, the usually employed methods for the calculation of unsteady heat transfer through walls are based on the hypothesis that such walls are composed of homogeneous layers. In this framework, a study of the dynamic thermal performance of insulated blocks is brought forth in the present paper. A finite-volume method is used to solve the two-dimensional equation of conduction heat transfer, using a triangular-pulse temperature excitation to analyze the heat flux response. The effects of both the type of clay and the insulating filler are investigated and discussed at length. The results obtained show that the wall front mass is not the basic independent variable, since clay and insulating filler thermal diffusivities are more important controlling parameters.

Keywords: building envelope; thermal inertia; hollow block; thermal pulse response

1. Introduction

Dynamic heat transfer performance of building envelopes has been extensively studied, being of fundamental importance in building thermal behavior. Different authors have reached very different conclusions in relation to the research methods, climatic conditions, and key performance indicators [1]. Yet, the only available method to evaluate the attitude of a building element to reduce the effect of the heat wave that flows through it is applicable only to homogeneous layers with sinusoidal temperature solicitation, as reported in References [2,3]. Thus, it is not suitable for the evaluation of blocks in which two-dimensional (2-D) and three-dimensional (3-D) effects on heat transfer are not negligible. Field studies have pointed out relevant differences between measured and simulated results, even in walls made of full blocks, probably due to mortar [4].

As far as homogeneous multilayered walls are considered, studies by Asan and Sancaktar [5], Asan [6], and Lakatos [7] have shown that wall thickness is the most relevant parameter for the time lag of heat wave flux, though wall composition is also important. These results seem to be congruent with the common assumption that a high mass per unit front area of a wall leads to a high time lag.

This is reflected in the terms used to describe dynamic heat transfer behavior such as thermal mass, and heavy/light wall [1].

Some preliminary studies on non-steady state heat transfer in hollow bricks have provided conflicting results. Some papers are concerned with the effective heat capacity of hollow blocks. Lacarrière et al. [8] found that the effective heat capacity per unit volume of a brick is of the same order of that of the solid part of the brick in an experimental study on the response of a single vertically perforated brick subjected to a step temperature change. On the contrary, Sala et al. [9], in an experimental study on the response of a three-layered wall made of a Expanded Polystyrene (EPS) insulating layer, a hollow brick layer, and a gypsum layer, subject to a triangular temperature-pulse, found that the effective heat capacity per unit volume of the brick was nearly half of that of the clay which the solid part of the brick consisted of. Moreover, Zhang and Wachenfeldt [10] calculated that the heat capacity per unit volume of the equivalent homogeneous layer was about two times that of the solid part of a slab with a cavity area fraction about 50%, through numerical simulations. Although some of these studies did not provide time lag response to temperature solicitation, data from Reference [8] implied an 80% reduction of time lag due to a 50% reduction in front mass.

Other papers provide heat flux response graphs from numerical simulations or experiments that allow to observe the time lag. Martín et al. [11] and the cited paper from Sala et al. [9] provided experimental results of triangular pulse temperature solicitation on multilayer walls containing hollow bricks. In the former, the time lag is 4.4 h with a 180-mm thick brick layer, while the latter presents a time lag less than one hour for a 40-mm thick brick layer. Zhang et al. [12] experimentally studied heat transfer through a 190-mm thick layer of lightweight aggregate concrete with vertical cavities of two different sizes. They have found a 4.4 h time lag with a 24-h period of sinusoidal solicitation that is similar to that found in Reference [11], with similar thickness but higher front mass and different solicitation. Moreover, Arendt et al. [13] numerically studied the influence of cavity size on time lag and decrement factor in a 300-mm thick clay brick. Their results show that there is a maximum in time lag and a minimum in decrement factor at an intermediate cavity concentration, which is at an intermediate front mass. Cianfrini et al. [14] showed that time lag is not straightforwardly dependent on front mass in insulated blocks, while it is so in some conventional bricks [15]. Thus, the dynamic heat transfer performance of a block may not be simply inferred from material properties and geometry.

Besides, the heat transfer rate through outer walls may be reduced by filling bricks cavities with insulating materials. This has been confirmed in steady state heat transfer by some experimental and numerical studies, such as those of Zukowski and Haese [16], Tang et al. [17], Pavlík et al. [18], and Bassiouny et al. [19].

In this framework, the aim of the present study is to point out which are the relevant parameters for the thermal inertia of insulated blocks. A two-dimensional numerical study was performed under the assumption that the investigated block is subjected to a triangular temperature pulse on one side while the other is kept at a constant temperature. Standardized B9 block was chosen among those reported in EN1745:2002 [20], as a simplification of the integration domain is possible. Moreover, as it has a high cavity fraction, the insulating material properties are predicted to be more relevant on overall behavior. Different insulating materials and clay properties are considered.

2. Mathematical Formulation

The reference masonry unit is depicted in Figure 1. The brick is made of clay, while the cavities are considered to be filled with three different insulating materials or the same clay. The simulation domain is limited to the central line of cavities, imposing adiabatic boundary conditions along the midlines of the ribs.

Triangular pulse excitation was used to check the dynamic heat transfer characteristics, applied to face S, as proposed in Reference [9]. This kind of solicitation allows us to evaluate the time lag as the delay between the peak of the temperature pulse and the peak of heat transfer on the other

side, as well as the decrement factor, which is the ratio of the actual peak heat transfer to that with constant temperature equal to the peak value, as defined in Reference [4], as depicted in Figure 2. A 10-K high, 2-h wide pulse was chosen. As stated above, adiabatic conditions were assumed along domain boundaries defined by the dashed lines, while the face N, which was not subject to the pulse, was kept at constant uniform temperature.

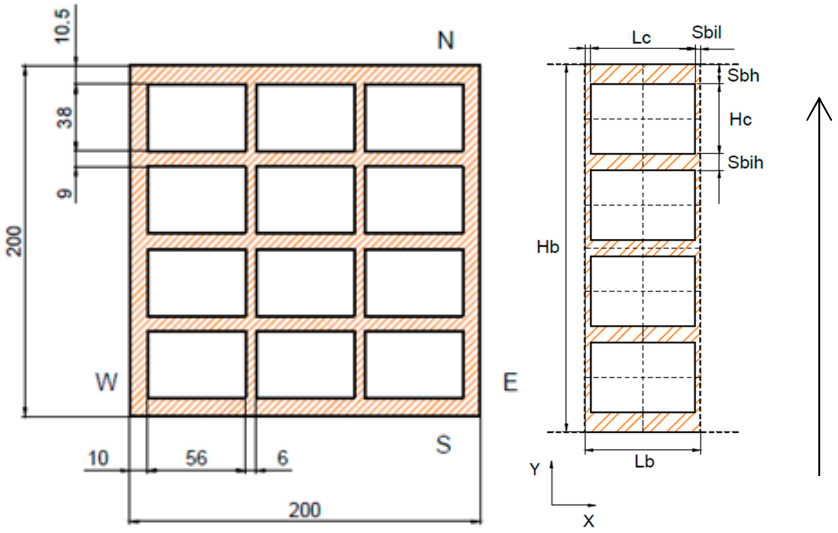

Figure 1. Sketch of the masonry unit and simulation domain; dimensions in mm; heat flux direction shown by the arrow.

The thermal field equation is described by a Cartesian two-dimensional Fourier's equation for conducting fields:

$$k\left(\frac{\partial^2 T}{\partial x^2}+\frac{\partial^2 T}{\partial y^2}\right)=c_p\rho\frac{\partial T}{\partial \tau} \tag{1}$$

where k stands for thermal conductivity, T for temperature, c_p for isobaric specific heat, ρ for density, and τ for time.

On surface N, a 20 °C uniform and constant temperature was imposed. On surface S, a uniform triangular pulse temperature was imposed:

- increasing from 20 °C to 30 °C with a 2.778×10^{-3} K/s (10 K/h) temperature increase rate in the period from time 0 s to time 3600 s;
- decreasing from 30 °C to 20°C with a -2.778×10^{-3} K/s (−10 K/h) temperature decrease rate in the period from time 3600 s to time 7200 s;
- constant at 20 °C for any time afterwards.

At the cavity boundary, heat flux conservation is given by:

$$k_a\left.\frac{\partial T}{\partial n}\right|_a=k_b\left.\frac{\partial T}{\partial n}\right|_b \tag{2}$$

where, besides the symbols used in Equation (1), n stands for direction perpendicular to boundary, either x or y, and subscripts a and b stand for the materials on the sides of the boundary.

A 20 °C uniform temperature in whole integration domain was used as an initial condition.

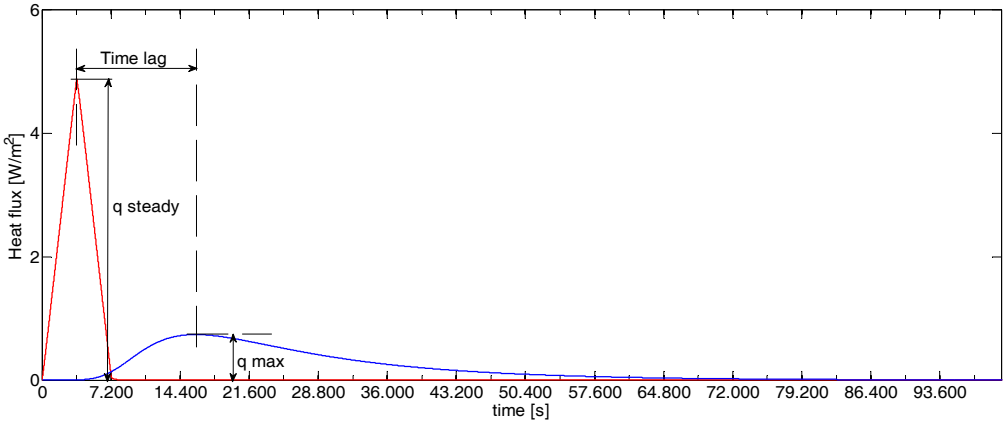

Figure 2. Equivalent steady state heat flux vs. actual heat flux for Expanded Perlite insulation in the light weight clay (LWC) block.

3. Computational Procedure

The governing equation was solved through a control-volume formulation of the finite-difference method, along with boundary and initial conditions stated above. A rectangular mesh was used, as sketched in Figure 3. A first-order backward scheme was used for time stepping. At inner nodes, the discretization of Equation (1) becomes:

$$\begin{aligned} T_P\left(\frac{(c_p\rho)_P\Delta x_P\Delta y_P}{2k_P\Delta\tau}+\frac{k_N\Delta x_P}{k_N\Delta y_P+k_P\Delta y_N}+\frac{k_S\Delta x_P}{k_S\Delta y_P+k_S\Delta y_N}+\frac{k_E\Delta y_P}{k_E\Delta x_P+k_P\Delta x_E}+\frac{k_W\Delta y_P}{k_W\Delta x_P+k_P\Delta x_W}\right) \\ -T_N\left(\frac{k_N\Delta x_P}{k_N\Delta y_P+k_P\Delta y_N}\right)-T_S\left(\frac{k_S\Delta x_P}{k_S\Delta y_P+k_S\Delta y_N}\right)-T_E\left(\frac{k_E\Delta y_P}{k_E\Delta x_P+k_P\Delta x_E}\right) \\ -T_W\left(\frac{k_W\Delta y_P}{k_W\Delta x_P+k_P\Delta x_W}\right)=\frac{(c_p\rho)_P\Delta x_P\Delta y_P}{2k_P\Delta\tau}\cdot T_P^{(\tau-1)} \end{aligned} \quad (3)$$

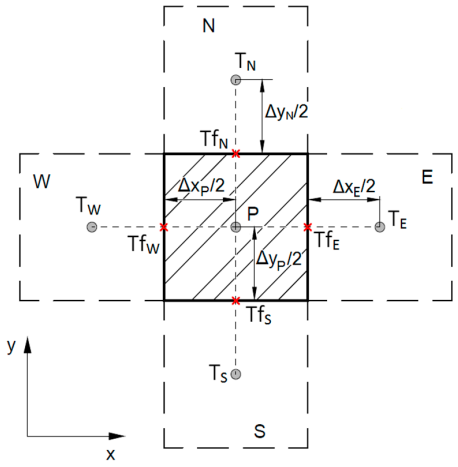

Figure 3. Discretization of the thermal field.

Equation (3) is adapted in boundary elements, imposing temperature values on Tf_N and Tf_S, or adiabatic boundary conditions, i.e., $Tf_E = T_P$ and $Tf_W = T_P$, whichever is relevant.

The discretized equations lead to a system of linear equations. The iterative Jacobi algorithm [21] was implemented to solve the system.

The average heat flux through face N (of length Lb) was calculated by integration, Equation (4). The temperature derivative was calculated by three-point backwards derivative. Integration was done by Trapezoid rule (first degree Newton-Cotes formula).

$$q = \frac{1}{Lb}\int_0^{Lb} k\frac{\partial T}{\partial y}dx \tag{4}$$

The code was checked against reference simple analytic solutions found in Reference [2]. Steady state 2-D fields were compared for a rectangular homogenous slab with adiabatic boundary conditions on three sides, and sinusoidal temperature on the fourth. Analytic solution of temperature field is given by Equation (5). Comparison of numerical solutions for different slab and mesh sizes are provided in Table 1, with very good agreement.

$$T(x,y) = T_{max}\frac{sinh\left(\frac{\pi y}{L_b}\right)}{sinh\left(\frac{\pi H_b}{L_b}\right)}sin\left(\frac{\pi x}{L_b}\right) \tag{5}$$

Table 1. Comparison of numeric solutions in steady state to Equation (5).

Lb (mm)	Hb (mm)	Nodes	Maximum Relative Difference of Temperature Field
40	105	40×105	3.00×10^{-3}
40	105	80×210	7.35×10^{-4}
105	40	105×40	2.78×10^{-5}
248	175	50×50	2.40×10^{-4}

Unsteady temperature fields were compared for a rectangular homogenous slab with adiabatic boundary condition on three sides, and step temperature change on the fourth, from 20 °C to 0 °C. Analytic solution of temperature field is given by Equation (6). Comparison between analytical and numerical solutions is shown in Figure 4. Relative temperature difference is lower than 4×10^{-4} for the 24-h long simulation, apart from the initial time steps.

$$T(y,\tau) = \frac{2}{H_b}T_0\sum_{n=0}^{\infty} e^{-\lambda_n^2\alpha\tau}.\frac{sin(\lambda_n H_b)}{\lambda_n}cos(\lambda_n y) \tag{6}$$

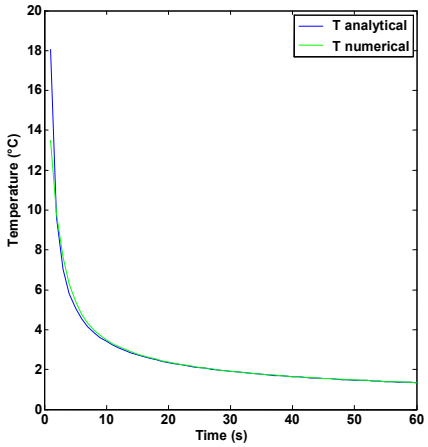

Figure 4. Comparison between analytical and numerical temperature solutions at the midplane of the slab for the first 60 s.

Moreover, a self-consistency test was conducted to determine the optimal mesh-size, time step, and variance limit for iterations. A 5-s time step and 10^{-4} variance limit were found to create a good balance between calculation time and solution accuracy with mesh sizes between 21×103 and 44×210, depending on the cavity number and geometry.

4. Results

Numerical simulations were performed for each kind of insulation filler, as well as for full blocks. Masonry material includes clay of three different densities. Insulating filling materials that are considered in present paper are Expanded Perlite, Mineral Wool, and Expanded Polystyrene. Properties of materials are given in Table 2. Properties of clay are provided in Reference [20] according to density. Properties of insulating materials come from datasheets available on manufacturers' websites.

Table 2. Properties of masonry and insulation materials. LWC: light weight clay; MWC: medium weight clay; HWC: heavy weight clay.

Material	ρ (kg/m^3)	c_p (J/kg K)	c_p*ρ (kJ/m^3 K)	k (W/m K)	α (m^2/s)
LWC	1000	1000	1000	0.27	0.27×10^{-6}
MWC	1700	1000	1700	0.51	0.30×10^{-6}
HWC	2400	1000	2400	0.84	0.35×10^{-6}
Expanded Perlite	16	1260	20.16	0.052	2.6×10^{-6}
Mineral Wool	265	800	212	0.049	0.23×10^{-6}
Expanded Polystyrene	40	1210	48.4	0.029	0.60×10^{-6}

Clay of maximum density (heavy weight clay (HWC)) shows a thermal conductivity circa three times higher than the lower density clay (light weight clay (LWC)). The thermal diffusivity of HWC is only 30% higher than that of LWC, as density compensates for thermal conductivity. All types of insulating materials have lower thermal conductivity and specific heat per unit volume than clay. On the contrary, the thermal diffusivity of insulating materials in comparison to clay is slightly lower for Mineral Wool, but almost double for Expanded Polystyrene and 10 times higher for Expanded Perlite. Notice that as all materials share similar specific heat, their heat capacity per unit volume is proportional to density.

For each simulation, heat transfer rate on face N is calculated from Equation (4). Time evolution of heat flux for block filled with Mineral Wool is depicted in Figure 5, with different clay density. All seem to share the same time lag despite having very different front masses.

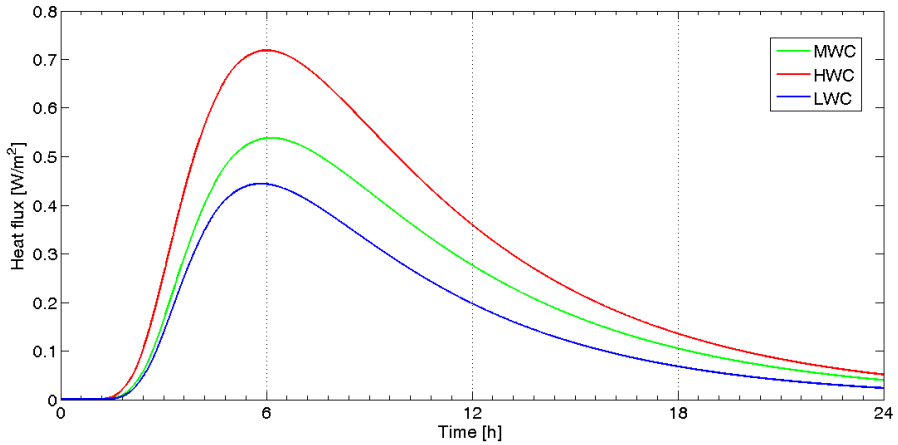

Figure 5. Heat flux vs. time for blocks filled with Mineral Wool and different clay densities.

Comparing time evolution of heat flux for blocks made of the same clay (HWC) but with different infill materials, larger differences in time lag were found, as shown in Figure 6. What is more evident is that although the full block has the highest front mass, it shows the least time lag.

Thus, for each configuration, the time lag ($\Delta\tau$) was calculated as the delay between the temperature peak on face S and the heat flux peak on face N, as well as damping degree, which is the reciprocal of the decrement factor.

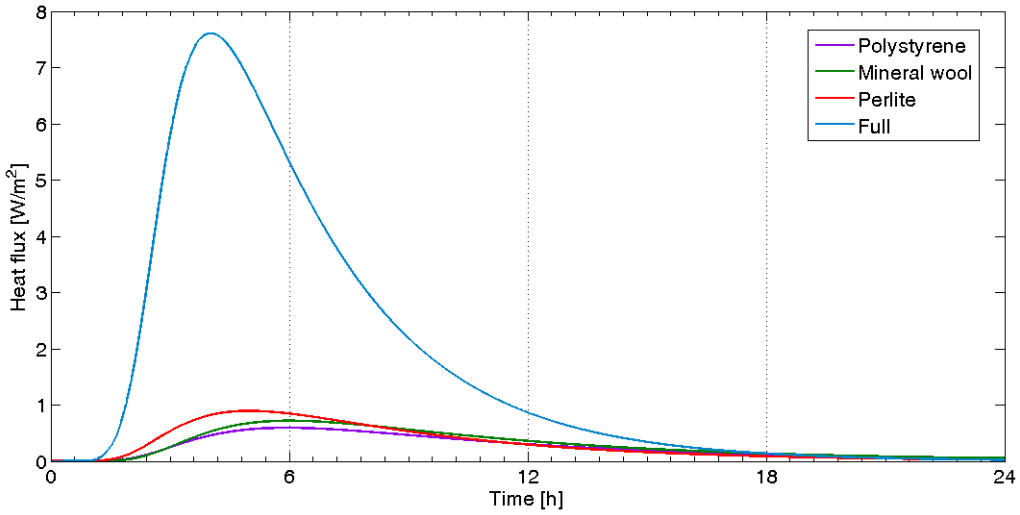

Figure 6. Heat flux vs. time for HWC blocks filled with different infill materials.

Time lags and damping degrees for different combinations of clay density and insulating material as well as full blocks vs. front masses of the block are plotted in Figures 7 and 8, respectively. It is evident that front mass is not directly linked to time lag nor to decrement factor.

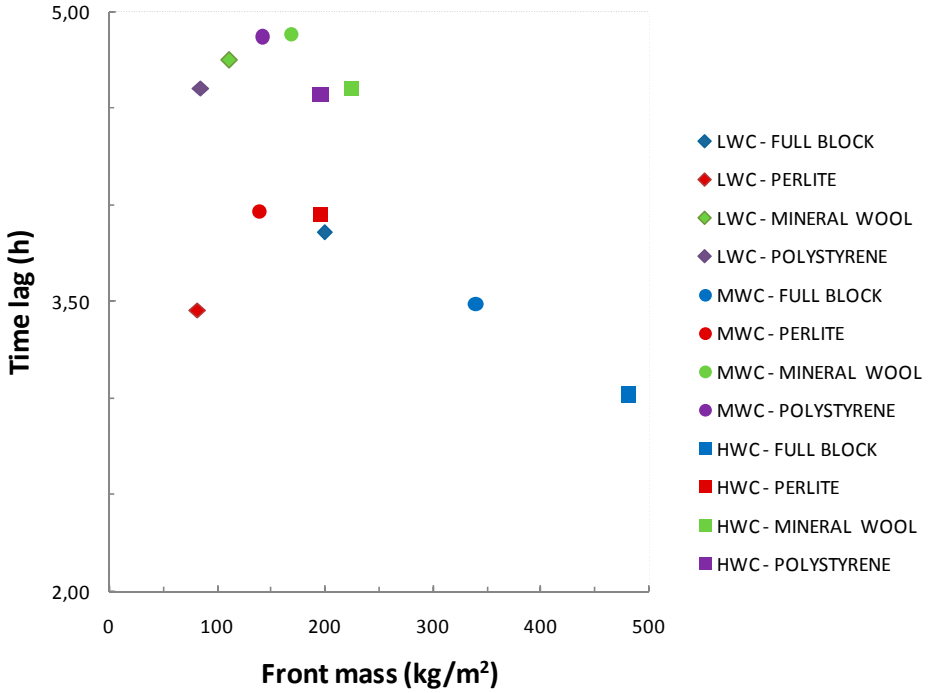

Figure 7. Time lag (in hours) vs. front mass, all material combinations.

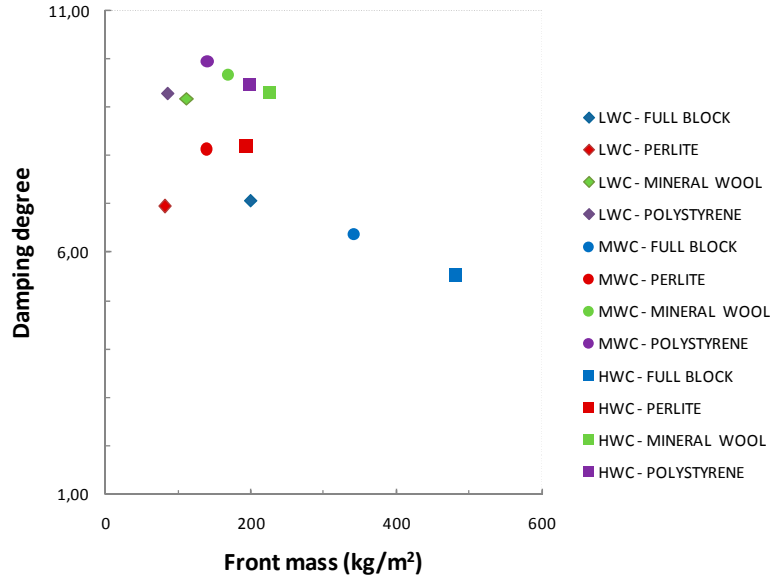

Figure 8. Damping degree vs. front mass, all material combinations.

5. Discussion

Results show that time lag is far from being linearly correlated to front mass. The highest time lag values were found for Mineral Wool insulated blocks. On the contrary, Expanded Perlite insulation, which has a much higher thermal diffusivity, showed lower time lags than other insulating materials.

The values in Figures 7 and 8 seem to have almost the same arrangement; thus, time lag was plotted versus damping degree, as shown in Figure 9. A linear correlation emerged between these two performance indicators.

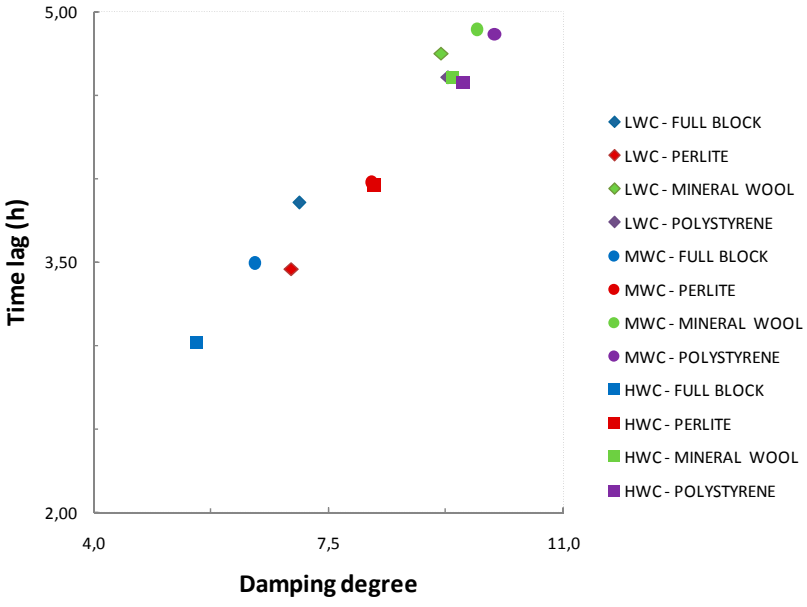

Figure 9. Time lag (in hours) vs. damping degree, all material combinations.

Full blocks showed a reverse correlation to front mass, as lighter clay provided higher time lags. In fact, clay density was found to be directly correlated to thermal diffusivity, so this might be relevant to predicting dynamic response to temperature solicitation.

Thermal diffusivity is the ratio of heat conduction to heat capacity per unit volume of a given medium. So, it is possible to define it as the ratio between equivalent thermal conductivity and specific heat per unit volume for a non-homogeneous block.

Equivalent thermal conductivity (k_{eq}) may be defined as the ratio of steady state heat flux per unit area (q_{steady}) multiplied by its thickness (Hb) to the temperature difference on its sides ($T_S - T_N$):

$$k_{eq} = \frac{q_{steady}\ Hb}{(T_S - T_N)}. \tag{7}$$

$$cv = \frac{\sum c_j\ \rho_j\ A_j}{\sum A_j}. \tag{8}$$

Moreover, it is possible to define the mean heat capacity per unit volume (cv) as the average of heat capacity per unit volume of each composing material weighted with its volume (area in a 2-D configuration):

The equivalent thermal diffusivity of a block is thus defined from Equation (9):

$$\alpha_{eq} = \frac{k_{eq}}{cv}. \tag{9}$$

Plotting time lag for the considered blocks against their equivalent thermal diffusivity, there emerged a clear correlation, as depicted in Figure 10. Plotting time lag values against the reciprocal of equivalent thermal diffusivity of each block showed a straight correlation, as depicted in Figure 11. Yet, full blocks and those insulated with Mineral Wool exhibited a steeper correlation compared to blocks insulated with high thermal diffusivity materials such as Expanded Polystyrene and Expanded Perlite. More materials and different blocks should be considered to provide enough data to propose a correlating equation that would be of any practical interest.

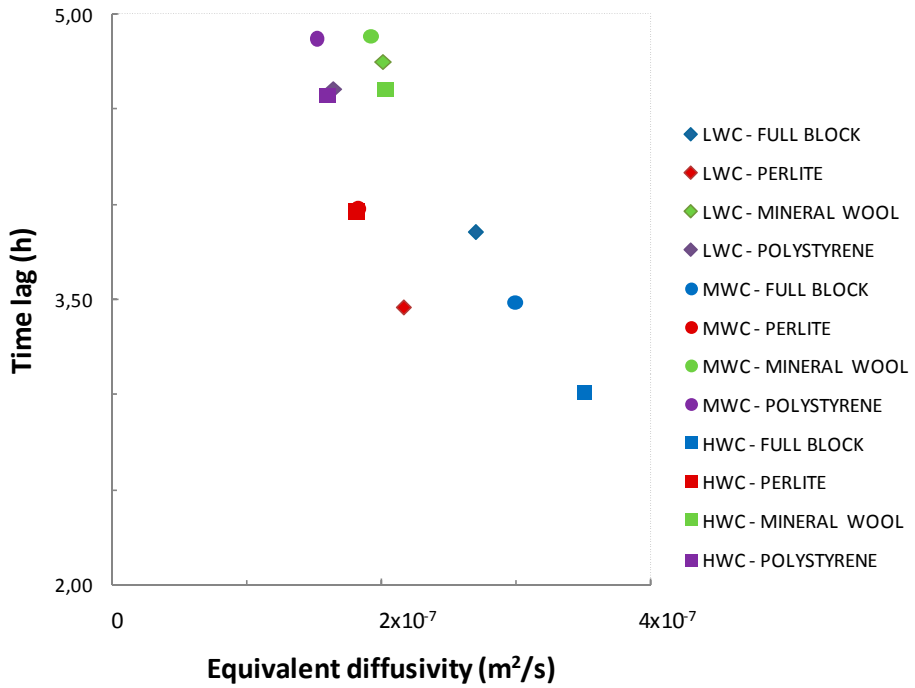

Figure 10. Time lag (in hours) vs. block equivalent diffusivity, all material combinations.

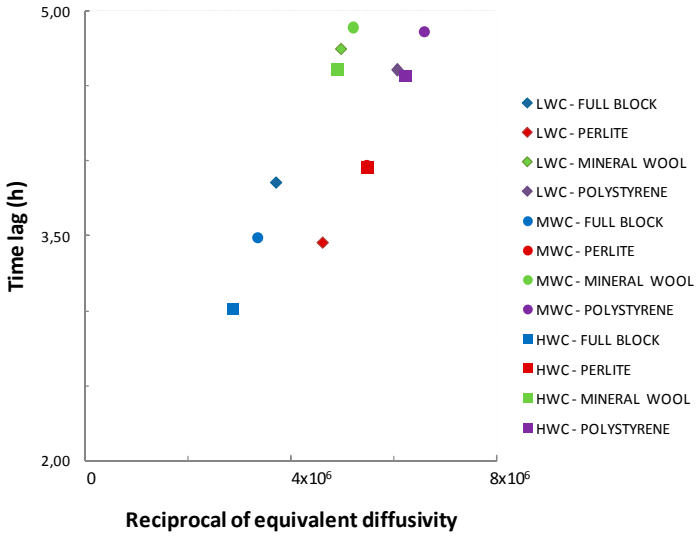

Figure 11. Time lag (in hours) vs. reciprocal of block equivalent diffusivity, all material combinations.

6. Conclusions

Heat transfer in blocks with different infill insulating materials has been numerically studied. Dynamic thermal features including time lag and decrement factor, in response to a triangular temperature pulse, have been analyzed. The influence of front mass on time lag that is implicit in common expressions such as "heavy walls" and "light walls", used to describe building performance in the open literature, has been found to be not correct. On the contrary, for some blocks, a lower front mass leads to a higher time lag.

Once the equivalent thermal diffusivity of blocks is defined, there is a straight correlation between time lag and the reciprocal of equivalent thermal diffusivity. Yet, there is some spreading of data due to insulating material thermal diffusivity.

Moreover, a linear correlation between damping degree and time lag has been found, thus further analysis should be focused on the latter in order to determine the dynamic thermal features of building components.

However, this is just a first approach to a wide field of research showing unexpected results. Much more work should be conducted in order to fully understand the unsteady behavior of hollow and insulated blocks, as block thickness is expected to play a relevant role.

Acknowledgments: This research did not receive any specific grant from funding agencies in the public, commercial, or not-for-profit sectors.

Author Contributions: Marta Cianfrini and Emanuele Habib conceived and developed the numerical code, Marta Cianfrini performed numerical simulations, Marta Cianfrini and Emanuele Habib analyzed the data, Roberto de Lieto Vollaro wrote the paper.

Conflicts of Interest: The authors declare no conflict of interest.

References

1. Verbeke, S.; Audenaert, A. Thermal inertia in buildings: A review of impacts across climate and building use. *Renew. Sustain. Energy Rev.* **2017**, in press. [CrossRef]
2. Carslaw, H.S.; Jaeger, J.C. *Conduction of Heat in Solids*, 2nd ed.; Clarendon Press: Oxford, UK, 1959; ISBN 0198533683.
3. International Organization for Standardization (ISO). *Thermal Performances of Building Components—Dynamic Thermal Characteristics—Calculation Methods*; ISO: Geneva, Switzerland, 1999; EN ISO 13786:1999.
4. Evola, G.; Marletta, L.; Natarajan, S.; Patanè, E.M. Thermal inertia of heavyweight traditional buildings: Experimental measurements and simulated scenarios. *Energy Procedia* **2017**, *133*, 42–52. [CrossRef]

5. Asan, H.; Sancaktar, Y.S. Effects of Wall's thermophysical properties on time lag and decrement factor. *Energy Build.* **1998**, *28*, 159–166. [CrossRef]
6. Asan, H. Numerical computation of time lags and decrement factors for different building materials. *Build. Environ.* **2006**, *41*, 615–620. [CrossRef]
7. Lakatos, A. Investigation of Heat Transfer Decrement of Wall Structures comparison of Measurements and Calculations. WSEAS Transactions on Heat and Mass Transfer. Available online: http://www.wseas.org/multimedia/journals/heat/2016/a025812-176.pdf (accessed on 8 November 2017).
8. Lacarrière, B.; Trombe, A.; Monochoux, F. Experimental unsteady characterization of heat transfer in a multi-layer wall including air layers—Application to vertically perforated bricks. *Energy Build.* **2006**, *38*, 232–237. [CrossRef]
9. Sala, J.M.; Urresti, A.; Martin, K.; Flores, I.; Apaolaza, A. Static and dynamic thermal characterization of a hollow brick wall: Tests and numerical analysis. *Energy Build.* **2008**, *40*, 1513–1520. [CrossRef]
10. Zhang, Z.L.; Wachenfeldt, B.J. Numerical study on the heat storing capacity of concrete walls with air cavities. *Energy Build.* **2009**, *41*, 769–773. [CrossRef]
11. Martín, K.; Flores, I.; Escudero, C.; Apaolaza, A.; Sala, J.M. Methodology for the calculation of response factors through experimental tests and validation with simulation. *Energy Build.* **2010**, *42*, 461–467. [CrossRef]
12. Zhang, Y.; Du, K.; He, J.; Yang, L.; Li, Y.; Li, S. Impact factors analysis on the thermal performance of hollow block wall. *Energy Build.* **2014**, *75*, 330–341. [CrossRef]
13. Arendt, K.; Krzaczek, M.; Florczuk, J. Numerical analysis by FEM and analytical study of the dynamic thermal behavior of hollow bricks with different cavity concentration. *Int. J. Therm. Sci.* **2011**, *50*, 1543–1553. [CrossRef]
14. Cianfrini, C.; Corcione, M.; Habib, E. Dynamic Thermal Features of Insulated Concrete Bricks. In Proceedings of the 7th HEFAT Conference, Antalya, Turkey, 19–21 July 2010; pp. 1065–1071.
15. Cianfrini, M.; Corcione, M.; de Lieto Vollaro, R.; Habib, E.; Quintino, A. Thermal Inertia of Hollow Wall Blocks: Actual Behavior and Myths. In Proceedings of the CISBAT 2015 International Conference on Future Buildings and Districts–Sustainability from Nano to Urban Scale, Lausanne, Switzerland, 9–11 September 2015; pp. 149–154.
16. Zukowski, M.; Haese, G. Experimental and Numerical Investigation of a Hollow Brick Filled with Perlite Insulation. *Energy Build.* **2010**, *42*, 1402–1408. [CrossRef]
17. Tang, D.L.; Li, L.P.; Song, C.F.; Tao, W.Q.; He, Y.L. Numerical Thermal Analysis of Applying Insulation Material to Holes in Hollow Brick Walls by the Finite-Volume Method. *Numer. Heat Transf. Part A Appl.* **2015**, *68*, 526–547. [CrossRef]
18. Pavlík, Z.; Jerman, M.; Fort, J.; Cerný, R. Monitoring Thermal Performance of Hollow Bricks with Different Cavity Fillers in Difference Climate Conditions. *Int. J. Thermophys.* **2015**, *36*, 557–568. [CrossRef]
19. Bassiouny, R.; Ali, M.R.O.; NourEldeen, E.H. Modeling the thermal behavior of Egyptian perforated masonry red brick filled with material of low thermal conductivity. *J. Build. Eng.* **2016**, *5*, 158–164. [CrossRef]
20. British Standards Institution (BSI). *Masonry and Masonry Products—Methods for Determining Design Thermal Values*; BSI: London, UK, 2002; EN 1745:2002.
21. Gori, L. *Calcolo Numerico*, 5th ed.; Edizioni Kappa: Roma, Italia, 2006; ISBN 8878907391.